



Dynamical Insights into the Mechanism of a Droplet Detachment from a Fiber

Journal:	<i>Soft Matter</i>
Manuscript ID	SM-ART-06-2018-001257.R1
Article Type:	Paper
Date Submitted by the Author:	20-Aug-2018
Complete List of Authors:	Ojaghlou, Neda; Commonwealth of Virginia, Department of Chemistry Tafreshi, Hooman Vahedi; Virginia Commonwealth University, Mechanical and Nuclear Engineering Bratko, Dusan; Virginia Commonwealth University, Department of Chemistry Iuzar, Alenka; Virginia Commonwealth University, Department of Chemistry



Journal Name

ARTICLE

Dynamical Insights into the Mechanism of a Droplet Detachment from a Fiber

Received Date,
Accepted Date

DOI: 10.1039/x0xx00000x

www.rsc.org/

Neda Ojaghloou,^a Hooman V. Tafreshi,^b D. Bratko^a and Alenka Luzar^{*a}

Quantifying the detachment behavior of a droplet from a fiber is important in many applications such as fog harvesting, oil-water separation, or water management in fuel cells. When the droplets are forcibly removed from hydrophilic fibers, the ease of detachment strongly depends on droplet volume and the rate of the process controlled by the applied force. Experiments, conducted on a ferrofluid under magnetic force, as well as continuum level calculations from fluid mechanics have so far been unable to resolve the time-dependent dynamics of droplet detachment and, most importantly, to assess the role of the applied force as the key determinant of the volume of the droplet residue remaining on the fiber after detachment. In the present work, we study the mechanism of water droplet detachment and retention of residual water on smooth hydrophilic fibers using Nonequilibrium Molecular Dynamics simulations. We investigate how the applied force affects the breakup of a droplet and how the minimal detaching force per unit mass decreases with droplet size. We extract scaling relations that allow extrapolation of our findings to larger length scales that are not directly accessible by molecular models. We find that the volume of the residue on a fiber varies nonmonotonically with the detaching force, reaching the maximal size at an intermediate force and associated detachment time. The strength of this force decreases with the size of the drop, while the *maximal* residue increases with the droplet volume, V , sub-linearly, in proportion to the $V^{2/3}$.

1 Introduction

The adherence to, and removal of droplets from cylindrical fibers underlie applications from fog harvesting^{1–4}, oil–water and oil–air separation^{5–8}, and water transport in fuel cells.^{9,10} In all these applications, the performance of the system depends on the conditions for the liquid release from, and the extent of retention by the fibers¹¹, and quantitative information about droplet–fiber interaction is of great value in designing a new product. The equilibrium shape of a droplet on fiber^{12–15} has been examined in reasonable depth in the literature.^{16,17} For droplets and fibers in the micrometer range, it is known that when the gravity effect is negligible, two topologically distinct droplet shapes occur: asymmetric clamshell and axially symmetric barrel conformations, depending on the droplet volume, the contact angle, and the fiber radius.¹⁷ Fiber roughness and fiber orientation can also have a significant effect on the equilibrium shape of droplet and wettability.^{18–20}

Motivated by various applications in the field of automotive engineering, e.g., removal of airborne oil droplets from the engine exhaust via the so-called coalescence filters, experimental studies have been conducted to measure the force required to detach a droplet from a fiber and to use that

information to estimate an allowable velocity for the flow of smoke through a filter.^{21–24}

Using continuum simulations, the equilibrium shape of an isolated droplet deposited on a fiber under the influence of an enhanced external body force has been determined recently by Ameri et al.²⁵ These authors incrementally raised the magnitude of the external body force applied to a droplet until no equilibrium shape/position could be obtained for the droplet on the fiber. They referred to the maximal force the droplet could sustain in an equilibrated state as the force of detachment and studied its dependence on fiber diameter, fiber roughness, fiber wettability, and droplet volume.¹⁸ The continuum simulations²⁵, however, could not resolve the time-dependent dynamics of droplet detachment, and more importantly, the volume of the droplet residue on the fiber. The latter is especially important from an industrial viewpoint as it affects the repeatability of the droplet separation processes. For instance, to increase the efficiency of fiber filters, the volume of the residue should be suppressed to prevent the clogging of the fiber network^{20,26,27}, while in water harvesting increasing the volume residue on the fiber arrays improves the net's efficiency.² The residual volume depends on the droplet volume, the contact angle, fiber radius, and the surface microstructure on the natural fiber.^{4,20,28} Despite the importance of knowing the amount of the residue on the fiber

^a Department of Chemistry, Virginia Commonwealth University, Richmond, Virginia 23284, United States. Tel: +1 (804) 828-3367; E-mail: aluzar@vcu.edu

^b Department of Mechanical and Nuclear Engineering, Virginia Commonwealth University, Richmond, Virginia 23284, United States

in engineering processes, only a few studies report on the volume of the residue on the fibers. For instance, Weyer et al.²⁹ investigated the droplet motion on the crossed fibers and demonstrated that, depending on the fiber diameter and volume of the droplet, a controllable liquid residue remained at the fiber nodes. Kim et al.²⁶ also studied the droplet impact on a thin fiber and suggested the mechanical model that predicted the residual water mass on the fiber with respect to the fiber radius and impact speed.

None of the previously reported studies, either experimental or computational, have discussed the detachment of a droplet from a fiber when the external force was stronger than the detachment force. Likewise, no study has yet reported the volume of the residue left on a fiber when the droplet was detached with a force stronger than the detachment force (e.g., the volume of the residue on a fiber when the velocity of the flow through a filter exceeded an allowable velocity).

In the present work, we study the mechanisms of droplet detachment and retention of liquid droplets through the atomistic molecular dynamic (MD) simulations. While valid insights could in principle follow from continuum simulations, our approach relies directly on input atomic and molecular forces rather than on experimental data for *presumably* invariant and uniform macroscopic properties such as the interfacial tensions, viscosity, drop's perimeter friction³⁰, and possibly line tension effects. We address the fundamental questions about the droplet size-dependence of the minimal force capable of detaching a droplet from the fiber, and the effects of droplet size and applied force on the amount of liquid residue left on the fiber after the detachment. Our modelling studies of the droplet breakup uncover a strongly nonmonotonic influence of external force, with the amount of residual water maximized under the intermediate force strengths whereas a complete or near-complete detachment of the droplet can be achieved in both extremes, with the applied force only slightly, or considerably exceeding the minimal force of detachment. We perform multiple MD simulations for water droplets on a smooth hydrophilic fiber at varied system sizes and extract scaling relations that enable extrapolation of our findings to larger length scales that are not directly accessible by molecular models. Because of its fundamental appeal and importance for applications, we hope the work will inspire experimental investigations and theoretical analyses of liquid retention and its control through varied stimuli for droplet detachment from the fibers.

2 Methodology

Force Fields. The model fiber was built with Visual Molecular Dynamic VMD package.³¹ It consists of a rigid carbon nanotube with radius $r_f = 6.4 \text{ \AA}$ or 12.8 \AA comprised of 4336 or 22503 Lennard-Jones (LJ) carbon atoms. The radius of the fiber is held fixed during the simulation. To avoid possible finite size effects, the fiber is periodically replicated along the x -direction.

We use the rigid extended simple point charge (SPC/E)^{32,33} potential to model the atomistic water droplet. The model has been used repeatedly in studies of capillary phenomena involving water because it offers satisfactory estimates for water surface tension and wettability for a variety of

materials.^{34–41} This potential consists of a smoothly truncated Coulomb potential acting between partial point charges on oxygen ($-0.8476e_o$) and hydrogen ($0.4238e_o$) atoms and an O-H distance 1 \AA and the H-O-H angle at 109.47° . Further, oxygen atoms also interact via Lennard-Jones potential (LJ). In all our atomistic simulations the water-fiber interaction is based on Lennard-Jones potential between the SPC/E water molecules and the fiber. The LJ strength was characterized by $\epsilon_{co} = 0.6639 \text{ kJ mol}^{-1}$ with cutoff radius 11 \AA .

When simulating a larger fiber, which requires bigger droplets to cover the same range of reduced volumes $V_r = V/r_f^3$, we use the coarse-grained, monatomic water (mW) model^{42,43} to reduce the computational cost. We selected this model because of its similar properties⁴² with the atomistic model (SPC/E) at room temperature⁴⁴ such as contact angle, surface tension, and work of adhesion.⁴⁴ The model does not feature electrostatic interactions associated with explicit hydrogen and oxygen atoms. Each mW water molecule behaves as a single site particle, which is interacting with its neighbours through a short-ranged potential designed to form a tetrahedral structure. The intermolecular potential is comprised of a sum of pairwise two-body term and three-body interactions that have the form of the Stillinger-Weber potential (SW)⁴². In the coarse-grained water model, the interaction between the water molecules and the fiber is modeled with the two-body SW⁴⁵ potential with the contact distance water-carbon $\sigma = 3.2 \text{ \AA}$. To start from barrel shape droplet, we considered $\epsilon_{c-mw} = 0.8158 \text{ kJ mol}^{-1}$ for carbon-mW interaction. All intermolecular forces in the mW model vanish at a distance $a\sigma$, where $a = 1.8$.⁴⁵

Simulation Details. The simulations start by placing a water droplet on a cubic lattice above the fiber positioned along the z axis of a cubic simulation box of size 300 \AA . During the equilibration, the droplet on the fiber reaches the symmetric equilibrium barrel shape. We considered seven sizes of water droplets composed of 2×10^3 , 4×10^3 , 6×10^3 , 8×10^3 , 10×10^3 , 13×10^3 , and 17×10^3 water molecules which were represented by the atomistic water model, SPC/E³³, on top of a rigid fiber with radius $r_f = 6.4 \text{ \AA}$. Based on volumes of the droplets, (V), and fiber radius r_f , the reduced volume of the system, V_r , varied from 250, 500, 750, 1000, 1250, 1500, and 2000. Depending on the size of the droplet, the total length of the simulation run varied from 2.5 to 5 ns.

For the simulations with a fiber with a radius of $r_f = 12.8 \text{ \AA}$, we used a coarse-grained Monatomic water (mW).^{42,43} By considering the same reduced volumes as with the atomistic droplets, the droplets comprised 1.7×10^4 , 3.4×10^4 , 5.2×10^4 , 6.9×10^4 , 8.7×10^4 , 10.4×10^4 , or 13.9×10^4 mW water molecules. Depending on the size of the droplet, the total length of the run varied from 5 to 10 ns.

All MD simulations are carried out by using the LAMMPS⁴⁶ package in NVT ensemble. The temperature is kept constant at 300 K using the Nose-Hoover thermostat⁴⁷ with a relaxation time of 0.2 ps. Verlet integration is used with time step 1fs for atomistic water and 5fs for coarse-grained water. Long range coulombic-PPPM Ewald Summation with 10^{-5} accuracy and periodic boundary conditions are used in all dimensions.

The detachment of a droplet from the fiber was studied by using Non-Equilibrium Molecular Dynamics (NEMD). In

numerical simulations, we used two approaches to apply the external force to the droplet. In the first approach, an external force was exerted on every molecule of a droplet, and its strength was increased gradually until the droplet detached from the fiber (Figure S1-a). In the second approach, after reaching the equilibrium state, a constant force was applied to every molecule in the droplet in a direction perpendicular to the fiber and remained constant during the simulation (Figure S1-b). Using sufficiently slow rate of force increase, the two methods yield consistent estimates of the minimum detachment force of the droplet. However, applying the constant force eliminates any concern about the appropriate rate of force escalation. We therefore mostly considered the second method using the constant force on the droplet. Depending on the force strength, the time necessary to observe the detachment varied from 50 ps to 2ns for the strong and weak forces, respectively. To accommodate large drops, we also increase the size of the box in the direction of the force applied to the droplet.

3 Results and Discussion:

3.1 Droplet equilibrium shape on a fiber

In Figure 1, we plot a morphology diagram for atomistic water droplets on a fiber with radius $r_f = 6.4 \text{ \AA}$ as a function of the reduced volume and the strength of water-fiber interaction. The squares and triangles represent the conditions where the equilibrated droplets are of clamshell or barrel shape, respectively. We have found that weak water-fiber interactions and small droplet volume favor the clamshell shape, while for strong water-fiber interactions and large droplet volume only the barrel shape is stable. With nanosized droplets on a smooth fiber, we do not observe a bistability of the two morphologies that has been reported with macroscopic droplets for a wide range of parameters.⁴⁸ Comparatively low barriers between the two configurations of the droplets on the nano-sized fiber rationalize the absence of the bistable regime in nanoscale systems.

3.2 Droplet behavior in the presence of an external force

Figure 2 shows consecutive snapshots from MD trajectories of the atomistic droplet in the presence of external forces. The force is applied in the direction perpendicular to the fiber. It can be seen (Figure 2-a) that for the weak force, the droplet shape transforms from symmetric barrel shape to asymmetric clam-shell conformation. When the force per molecule becomes strong enough, the droplet eventually detaches from the fiber, but a certain percentage of droplet mass can remain on the fiber (Figure 2-b).

When applying a strong force on the droplet, the droplet shape doesn't fully transition to the clamshell (Figure 2-c), and it can detach as a whole. Figure (2-e) shows another possible outcome of applying a strong force to the droplet. It can be seen from the front view that the droplet detaches before reaching the clamshell shape. The snapshots of the coarse-grained system with fiber radius $r_f = 12.8 \text{ \AA}$ are also added to Figure (2-d) for comparison. As can be seen in Figure (2-d), the

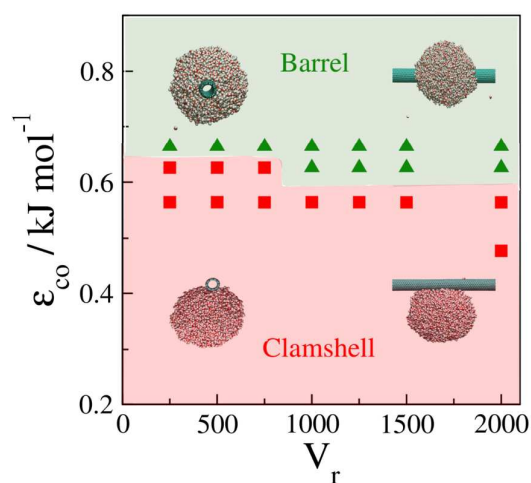


Figure 1. Morphology diagram of atomistic droplets deposited on a smooth fiber with fiber radius, $r_f = 6.4 \text{ \AA}$, at varied reduced volumes and water-fiber interactions. Green triangles denote the states where simulated droplets were consistently of stable barrel shape. Red squares show when the clamshell shape was stable. The threshold value of carbon-water interaction strength $\epsilon_{co} = 0.6 \text{ kJ mol}^{-1}$ corresponds to water-substrate contact angle $33^\circ \pm 3^\circ$, which could result in bistability in macroscopic systems. The number of water molecules corresponding to the given range of V_r varies from 2000-17000.

larger droplets considered by using the coarse-grained model detach faster from the fiber compared to the smaller ones represented by the atomistic model. The higher rates might also reflect to the differences in water diffusivities in the two models, with the diffusion coefficient of mW model 2.3 times greater than the one of the SPC/E model.⁴² The different diffusion constants reflect disparate viscosities of the two models, however, the relation between the detachment time and viscosity appears nonlinear⁴⁹, and it is not straightforward to renormalize the simulated detachment time to estimate the value corresponding to the experimental viscosity of liquid water.

To understand the breakup mechanism and determine the amount of residue of a nanoscale liquid droplet on the fiber, we perform multiple independent simulation runs. As illustrated in Figure S2(a-b), by applying the same force to the droplet, the amount of remaining water on the fiber varies from one simulation run to another. The variation of the residue size takes place because when a droplet stretches, it creates a narrow neck whose breakup position is subject to large fluctuations.⁵⁰⁻⁵² In figure S2 (c-e), we also illustrate the formation of a small satellite droplet emerging upon the breakup of the drop. In this case, the satellite droplet separated from the droplet after it detached from the fiber.

The visualization of the breakup trajectory revealed that the process of detachment from the fiber resembles the droplet breakup in the nano jet.⁵⁰⁻⁵² In these studies^{50,53,54}, thermal fluctuations at the nanoscale were identified as the major cause of irregular detachment. Even with fixed external force, these fluctuations occasionally produced multiple detachments. An example is provided in Fig. S2e illustrating a rare occurrence of satellite drops, however, we have not observed any consistent and reproducible multi-detachment pathways when applying a constant detaching force.

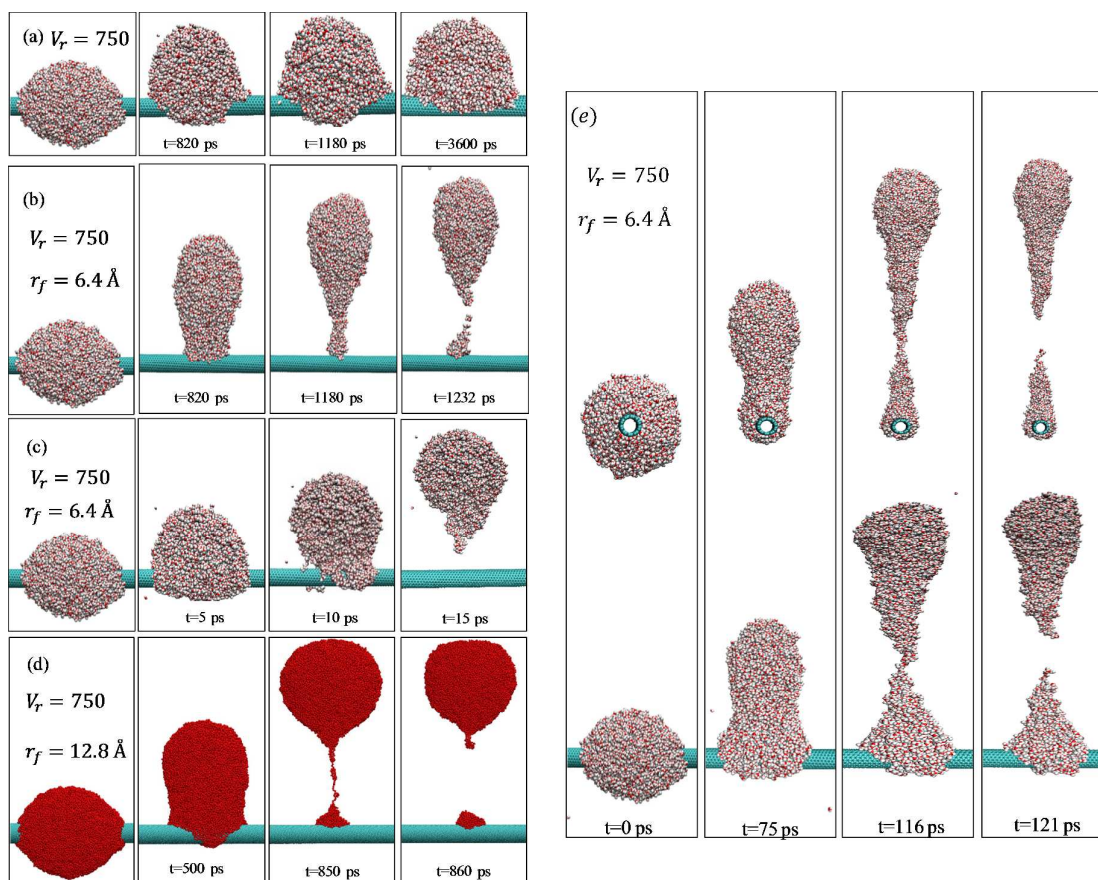
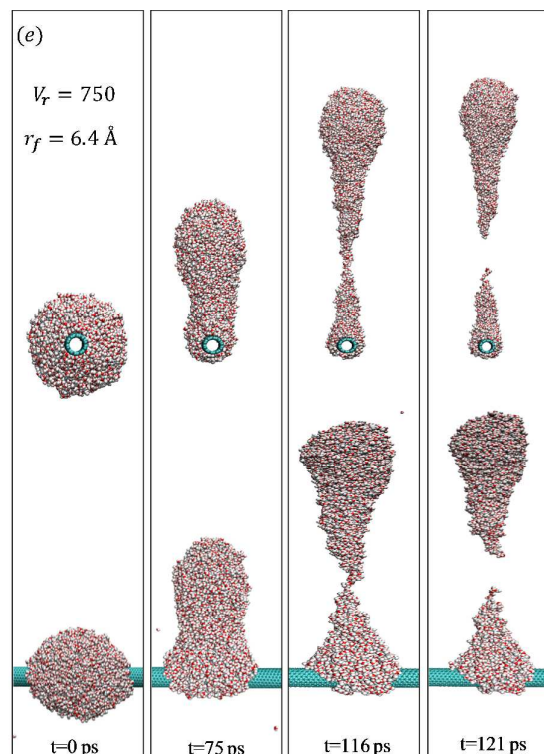


Figure 2. Snapshots from MD trajectories of the droplet detachment from fiber for the atomistic model and $V_r = 750$. Figures a-c illustrate the droplet evolution at different external forces, $F = 0.0041, 0.0058, \text{ or } 0.41 \text{ kJ mol}^{-1} \text{ \AA}^{-1}$ applied to the droplet in the direction perpendicular to the fiber. The atomistic droplet consists of 6000 SPC/E water molecules on the fiber with a radius $r_f = 6.4 \text{ \AA}$. Figure d presents snapshots from an MD trajectory of the droplet detachment from a fiber for a coarse-grained model at $V_r = 750$. The force exerted on the droplet was $F = 0.0016 \text{ kJ mol}^{-1} \text{ \AA}^{-1}$. The droplet consists of 52428 mW water molecules and the fiber radius is 12.8 \AA . Figure e, side view (bottom) and front view (top) snapshots from MD trajectories of the droplet detachment from fiber for the atomistic model with $V_r = 750$ and $F = 0.016 \text{ kJ mol}^{-1} \text{ \AA}^{-1}$, the force strength that maximizes the average residue on the fiber at given V_r .

Effect of droplet volume on the minimum detachment force.

Figure (3-a) shows the minimum force (per molecule) required to detach a droplet from a fiber ($r_f = 6.4 \text{ \AA}$) as a function of the reduced volume V_r . The minimum force per molecule of the liquid increases as the droplet volume decreases, in good agreement with the experiments²⁵ and continuum simulations for macroscopic droplets conducted using the Surface Evolver code.²⁵ As illustrated in the snapshots in Fig. 2, the detachment takes place after the nanodrop's shape transforms from the symmetric barrel shape to the asymmetric clamshell and the apparent contact angle of the droplet on the fiber approaches $\sim 90^\circ$. At this stage, the circumference of the droplet, C , shows only a weak dependence on the distance from the fiber. Upon further increase of the applied force, the droplet elongates, reaching the neck stage. As the neck narrows, the detachment process can proceed spontaneously even under a weaker force. By using this picture and by balancing the maximal capillary force $f_c \propto C\gamma$ ⁵⁵ and the external force acting on the droplet⁵⁶ $\rho FV \sim FR^3$, where V, ρ, γ are the droplet volume, the number density and surface

tension of the liquid, and R is the characteristic dimension of the droplet $R \propto V^{1/3}$, and by assuming C is roughly proportional to R , we can predict the variation of the force needed to detach the droplet with droplet size, $FR^3 \approx \gamma R \rightarrow F \propto 1/R^2 \propto V^{-2/3}$. Based on our estimate, increasing the volume of a droplet V from V_1 to V_2 decreases the minimum



detachment force of the droplet by the factor of $\left(\frac{V_1}{V_2}\right)^{2/3}$. In other words, the detachment force obtained for a specific reduced volume can be used to predict the force required to detach droplets of other sizes from the fiber. In Figure (3-a), the red curve represents the detachment force for

increased drop sizes as estimated by scaling the results for $V_r = 250$ in proportion to $V_r^{-2/3}$ for the atomistic system. This scaling prediction is in reasonable agreement with the simulation results.

The minimum detachment force for different fiber radii.

We have previously shown²⁵ that for a constant reduced volume V_r , increasing the fiber radius from the radius r_1 to radius r_2 , decreases the detachment force by a factor of $\left(\frac{r_1}{r_2}\right)^2$. This prediction also follows directly from our earlier observation that the minimum detachment force (per unit mass) varies as $V^{-2/3}$. If V_r is held constant, $V \sim r_f^3$, and

$F \sim r_f^{-2}$. In Figure 3-b, we validate this relation by comparing our simulation results for $r_f = 6.4 \text{ \AA}$ with additional results at the same reduced volume but larger fiber radius $r_f = 12.8 \text{ \AA}$. We rescale the results obtained with the larger fiber radius by multiplying the force by a factor of $\left(\frac{r_1}{r_2}\right)^2 = \frac{1}{4}$. Figure 3-b shows that the scaled results from fiber $r_f = 12.8 \text{ \AA}$ are in excellent agreement with simulation results of the fiber with radius $r_f = 6.4 \text{ \AA}$.

By applying the same concept, we rescaled the data from the previous work²⁵, which concerned drops and fibers in the μm range, to predict the detachment force at length scales of our atomistic model. Figure 3-b compares the detachment force obtained from MD simulations of the atomistic system with radius $r_f = 6.4 \text{ \AA}$ with those obtained by scaling the results for larger systems studied by MD coarse-grained simulations and Finite element simulations²⁵, with radii $r_f = 12.8 \text{ \AA}$, or $r_f = 107.5 \mu\text{m}$, respectively. The curves in Figure 3b show a good qualitative agreement; they could become essentially identical in the ideal scenario with precisely matched solid-vapor, solid-liquid, and liquid-vapor interfacial free energies of the two types of model systems. They also show that the proposed relation for the r_f dependence of the detachment force works well over the entire volume range. This observation gives strong support to the notion that the scaling behaviour observed with nano sized models is equally applicable to their macroscopic counterparts.

Effect of adhesion strength on the minimum detachment force. To check how the adhesion strength might affect the detachment force, we considered two different water-fiber interactions $\epsilon_{co} = 0.625 \text{ kJ mol}^{-1}$ and $\epsilon_{co} = 0.564 \text{ kJ mol}^{-1}$ corresponding to contact angles on flat surfaces in the absence of line tension effects, 30° and 50° .^{36,57,58} Figure 3-c shows the detachment force from MD simulations of the atomistic systems with radius $r_f = 6.4 \text{ \AA}$, compared to the results for larger systems previously characterized in experiment (detachment of aqueous ferrofluid droplets on the fishing line under magnetic field)²⁵ and Finite Element simulations²⁵, with fiber radius $r_f = 107.5 \mu\text{m}$ and contact angles $\theta = 30^\circ, 50^\circ$. As we are comparing systems with orders of magnitude different sizes, again, we rescaled the forces observed in the macroscopic and nanosized systems by the ratio of fiber diameters squared. Upon renormalization to nanoscale (Figure 3-c left), or macroscopic fiber dimensions (Figure 3-c right), the detachment forces from macroscopic experiments (violet stars in Fig. 3c) are indeed of the same order of magnitude as those deduced from simulations although the contact angle in the experimental system²⁵ remains only approximately known. Comparing the data for different contact angles shows easier detachment when the fiber is made more hydrophobic. The effect of adhesion strength (contact angle) diminishes with increasing V_r . Systematic simulations of minimal detachment forces for a range of fiber materials with varied adhesion strength, complementing recent measurements of its effect on the minimal detachment force⁴⁹, are being considered for future work but are outside the scope of the present project.

3.3 Droplet residue on a fiber

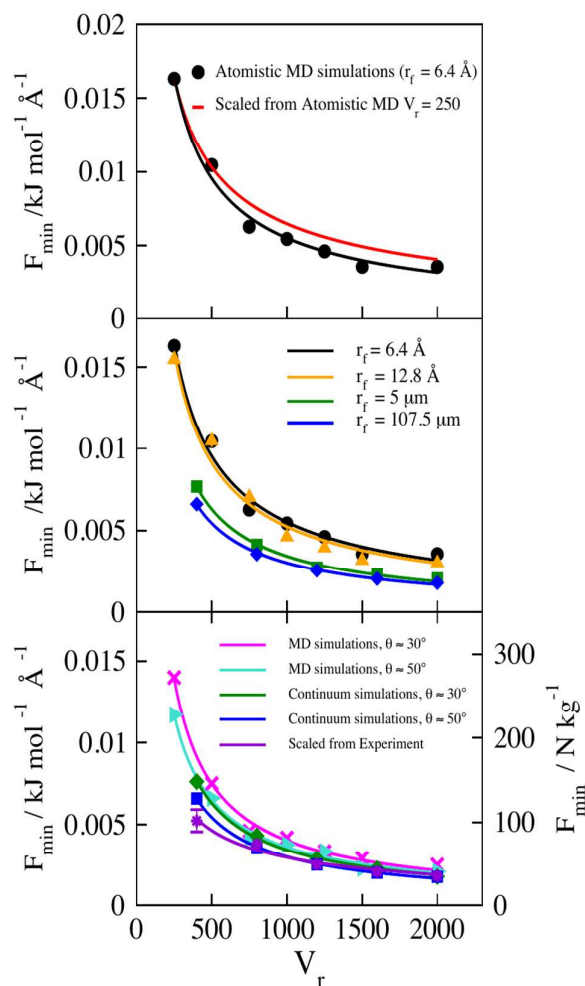


Figure 3. The minimum force required to detach the droplet from a fiber at different reduced volumes. a: the black symbols and curve describe simulation results of the atomistic model with the fiber radius 6.4 \AA . The red curve was produced by extrapolating the result for $V_r = 250$ in proportion to $V_r^{-2/3}$. b, black circles: atomistic simulations for fiber radius $r_f = 6.4 \text{ \AA}$; orange triangles: coarse grained system and fiber radius 12.8 \AA , rescaled to $r_f = 6.4 \text{ \AA}$; blue diamonds and green squares: data from the finite element simulations with two different fiber radii $5 \mu\text{m}$ and $107.5 \mu\text{m}$ ²⁵ rescaled to $r_f = 6.4 \text{ \AA}$. The latter two curves correspond to a bigger contact angle of water on the fiber $\theta \sim 50^\circ$.²⁵ c: results for fiber-water interaction strengths $\epsilon_{co} = 0.625 \text{ kJ mol}^{-1}$ and $\epsilon_{co} = 0.564 \text{ kJ mol}^{-1}$. Contact angles of atomistic water on flat surface with the same interactions are $\approx 30^\circ$ and 50° , respectively. The pink "x" and cyan triangles represent the force required to detach a droplet from a fiber with radius 6.4 \AA , for an atomistic model system with different water-fiber interactions. The remaining three sets of data (violet, green, and blue) correspond to macroscopic systems with $r_f = 107.5 \mu\text{m}$, rescaled to $r_f = 6.4 \text{ \AA}$. The violet stars describe experimental points²⁵ and the blue square and green diamonds are from finite element simulations with contact angles $30^\circ, 50^\circ$, respectively.²⁵ The right axis corresponds to the actual experimental and continuum simulation results for $r_f = 107.5 \mu\text{m}$, as well as the MD results obtained using $r_f = 6.4 \text{ \AA}$ and subsequently rescaled to $r_f = 107.5 \mu\text{m}$. Error bars are of the same size as the symbols.

In Figure 4, we plot the morphology diagram obtained from the atomistic simulations of water droplet deposited on the fiber with radius $r_f = 6.4 \text{ \AA}$, in terms of the control parameters such as the force and the reduced volume. The red line shows the minimum force of detachment, and the green color represents the threshold force, beyond which no residue of the droplet remains on the fiber. The three distinct regimes separated by these lines correspond to no detachment, partial detachment, or complete detachment of the droplet from the

fiber. In the first regime, the force is too weak to compete with cohesive forces in the droplet or the adhesion between the fiber and the droplet. Thus, the droplet does not detach from the fiber. When the external force is sufficient to overcome the surface tension, the droplet starts to elongate and eventually detaches. At an intermediate stage, the droplet stretches slightly and creates a neck. As the neck elongates and narrows, the breakup can happen at varying distances from the fiber.

Depending on the strength of the external force and the breakup position of the neck, a small fraction of the droplet can remain on the fiber. If the external force is very strong, it can prevail over the adhesion forces and the droplet detaches as a whole. Figure 4 also shows that the threshold force required for *complete* detachment increases with increasing droplet volume. Therefore, it is harder to detach the larger droplet entirely from the fiber.

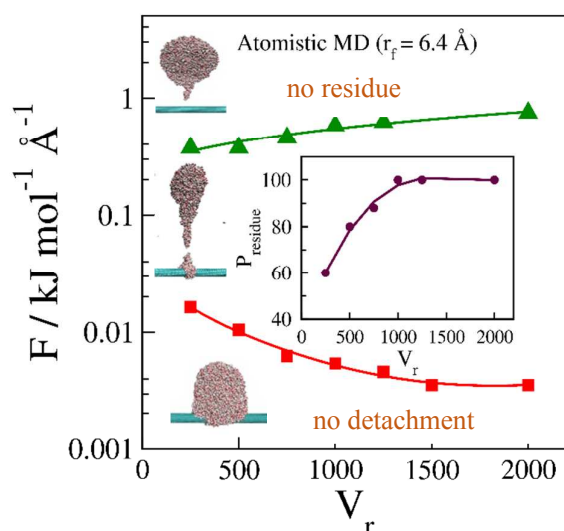


Figure 4. Morphology diagram of nano-sized droplets on a fiber with radius $r_f = 6.4 \text{ \AA}$, and $\epsilon_{co} = 0.6639 \text{ kJ mol}^{-1}$, over a wide range of applied forces F and reduced volume of the drop, V_r . The red color indicates the minimum force of detachment and green color indicates the threshold force above which no residue of the droplet remains on the fiber. The number of water molecules in a droplet varies from 2000 to 17000. The inset shows the probability P_{residue} of observing a residue on the fiber vs reduced volumes.

The inset in Figure 4 shows the probability of observing a residue after detachment in our simulations when applying the minimum detachment force. Here, the residue is considered to exist for any nonzero number of water molecules N_r remaining on the fiber. For the small fiber radius $r_f = 6.4 \text{ \AA}$, the probability of seeing the residue increases by increasing the reduced volume and reaches 100% for droplet sizes V_r exceeding $\sim 10^3$. For a wide range of intermediate force strengths, the average outcome is a partial detachment. Depending on the strength of the external force, a small portion of the droplet can remain on the fiber. When the force is close to the minimum detachment force, the droplet shape transforms from symmetric barrel shape to asymmetric clam-shell conformation before detaching from the fiber. For strong forces, the droplet does not have enough time to transform into the clam-shell configuration completely. This means that

the shape relaxation time (τ), of the droplet on the fiber in the presence of external forces exceeds the detachment time of the droplet. In order to find the relaxation time of the droplet, we determined the time correlation functions for the height of the center of mass, $R(t)$:³⁰

$$R(t) = \frac{\langle h(t) - h(\infty) \rangle}{\langle h(0) - h(\infty) \rangle}$$

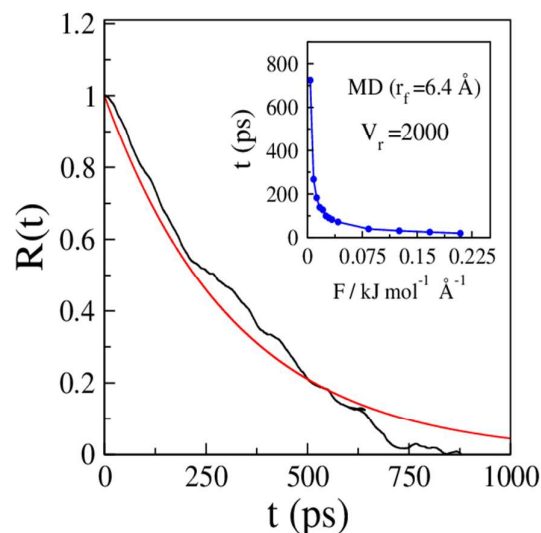


Figure 5. Time correlation function, $R(t)$, of the height of the center of mass of droplet on fiber for an atomistic system with reduced volume $V_r = 2000$ and fiber radius, $r_f = 6.4 \text{ \AA}$. At time close to 1ns, $R(t)$ crosses to the negative value due to inertia. The inset figure shows the detachment time of the droplet as a function of applied force. The red line shows an exponential fit to the simulated data.

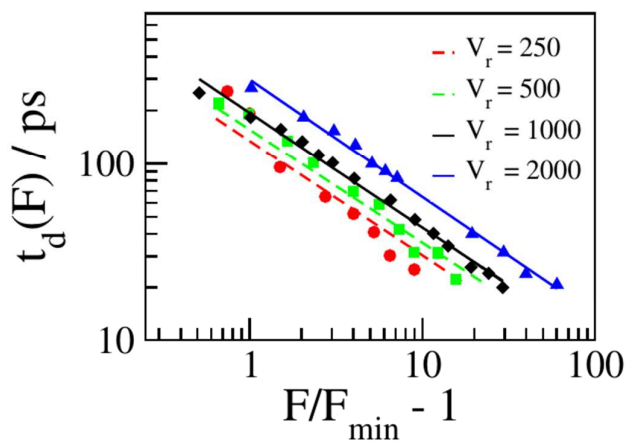


Figure 6: Symbols: MD detachment times of water droplets from the fiber of radius 6.4 \AA as functions of the relative excess of applied forces of strengths well above the minimal detachment force F_{min} (Fig. 3a) for the atomistic model of water. Scaling of the form $t_d \propto (F/F_{\text{min}} - 1)^{-2/3}$ is indicated for all droplet volumes above the smallest size ($V_r \sim 250$) where only approximate compliance is observed. Lines are fitted to the MD data using the fixed slope $-2/3$.

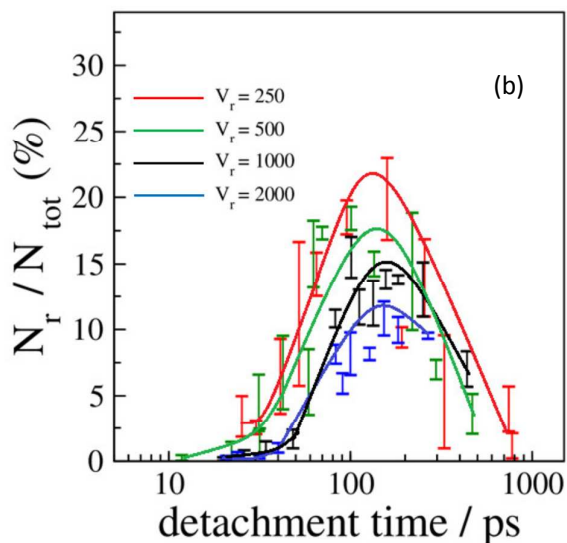
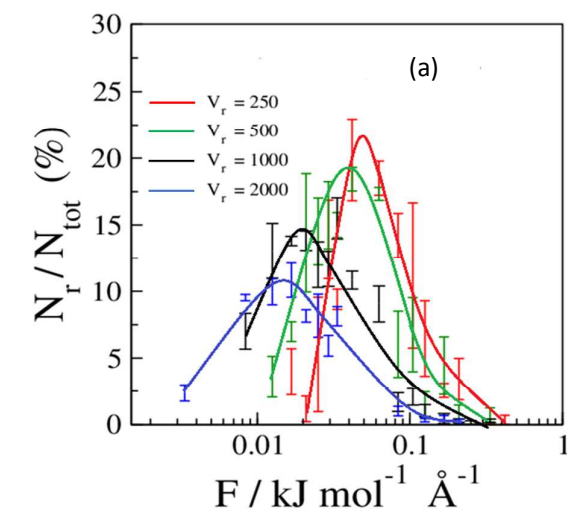


Figure 7. a: percentage of the residue of a droplet remaining on the fiber, $r_f = 6.4 \text{ \AA}$, obtained by applying a range of forces. The curves start at the minimum force of detachment. Error bars are estimated from multiple simulations for respective forces with each system statistically independent from others. b: percentage of the residue of the droplet on the fiber versus the detachment time.

following a change of the applied force acting on the drop. Above, $h(t)$ is the height of the center of mass of the droplet as a function of time. $h(0)$ is the initial height of the center of mass corresponding to the equilibrium shape of the droplet on the fiber under initial force $F=0.0016 \text{ kJ mol}^{-1} \text{ \AA}^{-1}$, and $h(\infty)$ the equilibrium height of the center of mass of the droplet, under the increased force $F=0.0025 \text{ kJ mol}^{-1} \text{ \AA}^{-1}$. Figure 5 illustrates the relaxation of an atomistic droplet on the fiber of radius $r_f = 6.4 \text{ \AA}$ and the reduced volume $V_r = 2000$. Assuming approximately exponential decay, the relaxation time $\tau \approx (0.36 - 0.4) \text{ ns}$, while the detachment time, (t_d), at maximal residue is $t_d \approx (0.135 - 0.185) \text{ ns}$. This result can be used to estimate relaxation times of droplets of different sizes. Recent experiments support the scaling of droplet relaxation time with volume $\tau \propto V^{1/3}$ ^{59,60}. The inset in Figure 5 illustrates the dependence of the detachment time of the droplet on the applied force. MD results for detachment times at applied forces well above the minimal detaching force F_{\min} (collected in Fig. 6) suggest an empirical scaling of the detachment time with the relative excess in the external force above the minimal detachment value, $t_d \propto [(F-F_{\min})/F_{\min}]^{2/3}$. At forces significantly stronger than the minimal detachment force, the detachment takes place before the transition to the clam shell shape could be completed and the process results in a larger residue on the fiber.

Soft Matter

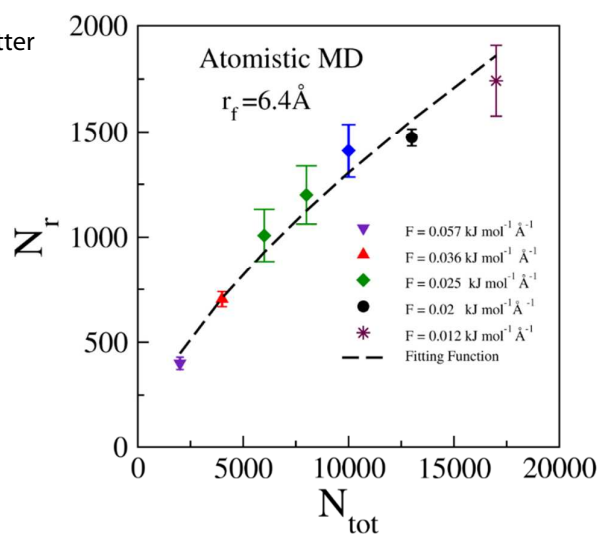


Figure 8. The average number of water molecules remaining on the fiber versus the total number of water molecules at detachment forces producing the maximal residue. The symbols denote the maximum residue on the fiber with radius 6.4 \AA at the time of detachment obtained from atomistic MD simulations. The dashed line indicates the fitting function $N_r \propto N_{tot}^{2/3}$ that is predicted by observing that the maximum residue corresponds to the double-cone pinch-off form⁶¹ of the detaching droplet (Fig 8).

To get a better insight into the water retention after the droplet detachment from the fiber, we compute the average amount of residue on the fiber from atomistic MD simulations under the minimum force of detachment for a range of droplet sizes from 2000 to 17000 water molecules on the fiber with radius $r_f = 6.4 \text{ \AA}$ or 12.8 \AA . We find out that the ratio of the number of retained water molecules, (N_r), to the total number of molecules in the droplet, (N_{tot}), never exceeds 10% when the minimum detachment force is applied.

We proceed by extending these calculations to stronger forces and determine the average residue size as a function of the applied force and the associated detaching time for a set of reduced volumes V_r . Our simulations provide the first quantitative insight into the residue dependence on droplet volume and applied force strength.

Figure 7a shows the percentage of the residue of a droplet on the fiber for different detachment forces obtained with the atomistic water model. At all droplet sizes, the residue on the fiber initially increases with the force until it reaches the maximum and then it decreases and eventually vanishes at very strong forces. The maximum amount of residue is never reached by applying the minimum detachment force. As we mentioned earlier, the initial increase of the residue size with the force is due to the fact that, at stronger forces, the droplet does not have enough time to transform entirely from the barrel shape to the clamshell shape (Figure 2e). Therefore, the detachment occurs when the fiber is still wetted over a larger area than in the clam-shell conformation. It should also be noted that as the droplet size increases, the maximum residue occurs at weaker forces. We also monitored the detachment time for the different reduced volume. As can be seen in Figure

(7-b), the volume of the residue on the fiber is small or negligible if the detachment is very slow or vary rapid, with the maximal average size obtained at an intermediate detachment time. To the best of our knowledge, this interesting behavior has not been previously reported.

To illustrate the dependence of the amount of the remaining water on the detachment force and the size of the droplet, in Figure 8 we plot the number of water molecules N_r in the maximal residue on the fiber versus a total number of water molecules on the droplet (N_{tot}) for different detachment forces. The maximal residue (at system-dependent force strengths F_{max} corresponding to the maxima in Fig. 7a) increases with the droplet size. The increase of N_r with N_{tot} is, however, sublinear; while the absolute residue increases with the droplet size, the fraction of residual water decreases with N_{tot} .

Figure 9 shows typical breakup configurations of the droplet under detaching forces yielding the maximal residue. The breakup profiles of the droplet at these conditions resemble two cones joined at their apexes (called the double cone profile)⁶¹ and lead to approximately symmetric pinch-off. The above shape emerges when the relaxation time of the droplet is longer than the detachment time. The detachment therefore occurs before reaching the clamshell shape. Since the residue approximately corresponds to the volume of the lower cone, $V_{LC} \sim \text{base area} \times \text{height} \sim (R \times r_f) \times R$ (R is the characteristic dimensions of the droplet $\sim V^{1/3}$), we find $V_{LC} \sim R^2 \sim V_{tot}^{2/3}$. Figure 8 confirms that our simulation results for the maximum residue of water after detachment from fiber follow the above prediction. Using the relationship $V_{res} \propto V_{tot}^{2/3}$ can help us to predict the volume of the residue on a fiber for different droplet volumes. Figure 10 shows the force that produces the maximal residue F_{max} on the fiber ($r_f = 6.4 \text{ \AA}$) versus reduced volume, V_r . F_{max} increases with decreasing the reduced volume V_r . The dashed line indicates the fitting function of the F_{max} versus V_r with the form $F_{max} = \text{const} \times V_r^{2/3}$. Our simulation results indicate that the force of the maximum residue varies according to the relation $F_{max} \sim V_r^{-2/3}$, in analogy to the minimum detachment force discussed in section (3.2). While our analysis concerns detachment events induced by gravity-like body forces, other types of perturbation, notably shear forces, can be of comparable practical importance and will be considered in planned future studies.

Conclusions

We have presented a comprehensive study aimed at predicting the external force required to detach the droplet from a smooth fiber through a combination of atomistic and coarse-grained Molecular Dynamics (MD) simulations. We have identified three regimes corresponding to no detachment, partial detachment, or complete detachment upon applying the external force perpendicular to the fiber. The outcome critically depends on the strength of the applied force, as demonstrated in the morphology diagram in Fig 4. Our results show that the minimum force (per molecule) capable of detaching a droplet from the fiber decreases with increasing volume of the droplet, in good agreement with experiments and continuum simulations for macroscopic droplets.²⁵ The results for the detachment force obtained for a system with droplet volume V_1 can be used to predict the detachment force for other droplet sizes V_2 according to the scaling relation $F_2 = F_1 \left(\frac{V_1}{V_2} \right)^{1/3}$.

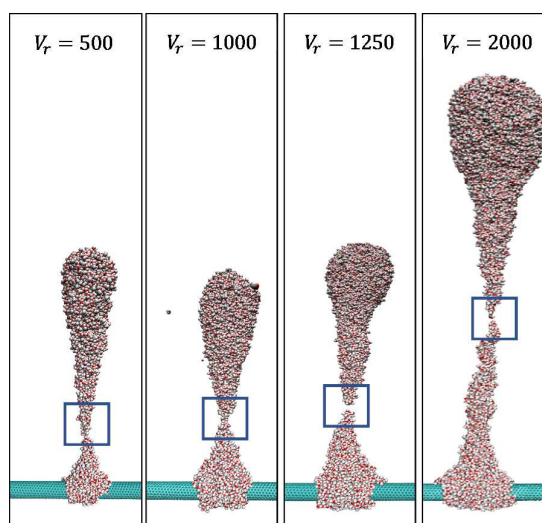


Figure 9. Snapshots of MD trajectories of the droplet at the time of detachment from the fiber for the atomistic model with fiber radius, $r_f = 6.4 \text{ \AA}$, when the residue is maximized. The droplet sizes vary from 4000, 8000, 10000, 17000 SPC/E water molecules.

We also computed the amount of the residue on the fiber after detachment for different droplet sizes and external forces. We observed that as the droplet size increases, a larger residue remains on the fiber, however, the fraction of the residual liquid expressed relative to the size of the droplet

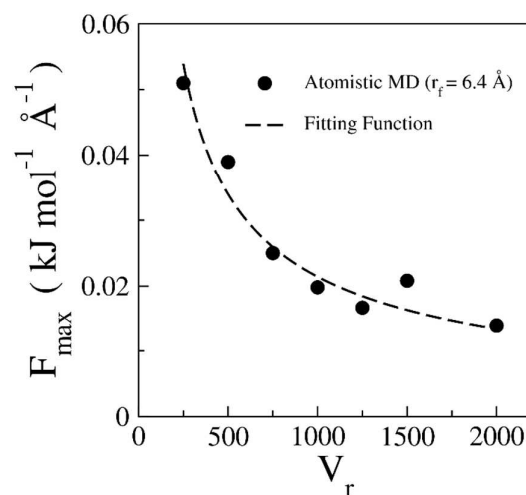


Figure 10. The force producing the biggest average residue, F_{max} on the fiber as a function of the reduced volume. The dashed curve indicates the fitting function $V_r^{-2/3}$. The droplet sizes in atomistic simulations vary from 2000 to 17000 SPC/E water molecules.

decreases with its size. The magnitude of the residue shows a nonmonotonic dependence on the applied force and concomitant detachment rate. While the entire droplet can be detached at sufficiently strong forces, and an almost complete detachment takes place at forces slightly above the minimal detaching force, we observe maximal residues at an intermediate force a few times stronger than the minimal detaching force. Within a broad range of system sizes we considered, the ratio of the two forces remains essentially

invariant with respect to the volume of the drop. Another useful insight of this study is the possible prediction of the maximal residue size from the prevalent geometry in the pinch-off state. By considering the breakup profile of the splitting droplet upon detachment, we predicted the maximum residue on the fiber to increase with the droplet volume V sub-linearly, in proportion to the $V^{2/3}$ and we confirm this dependence in explicit calculations. Our molecular simulations offer direct guidance for the control of liquid retention through external force and can provide the necessary input toward the development of methodologies for time-dependent continuum-level simulations at macroscopic scales relevant to industrial problems.

Conflicts of interest

There are no conflicts to declare.

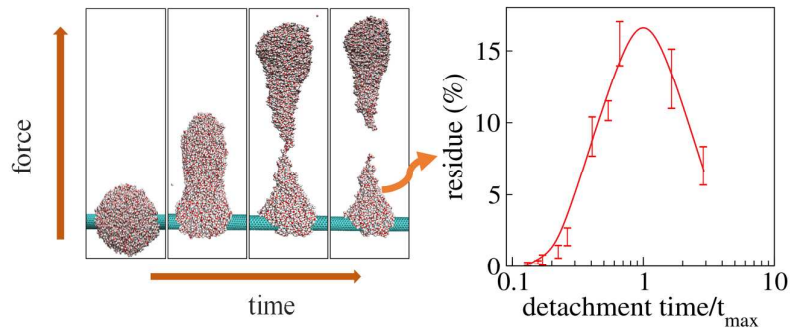
Acknowledgements

NO, HVT, and AL acknowledge support from the Presidential Research Quest Fund (PeRQ) award. DB thanks for partial support from the Office of Basic Energy Sciences, Chemical Sciences, Geosciences, and Biosciences Division of the U.S. Department of Energy under Grant No. DE-SC 0004406. This research used computing resources of the Extreme Science and Engineering Discovery Environment (XSEDE) supported by the National Science Foundation (Grant No. OCI-1053575).

References

- J. Ju, H. Bai, Y. Zheng, T. Zhao, R. Fang and L. Jiang, A multi-structural and multi-functional integrated fog collection system in cactus, *Nat. Commun.*, 2012, **3**, 1247.
- K. C. Park, S. S. Chhatre, S. Srinivasan, R. E. Cohen and G. H. McKinley, Optimal design of permeable fiber network structures for fog harvesting, *Langmuir*, 2013, **29**, 13269–13277.
- W. Shi, M. J. Anderson, J. B. Tulkoff, B. S. Kennedy and J. B. Boreyko, Fog Harvesting with Harps, *ACS Appl. Mater. Interfaces*, 2018, **10**, 11979–11986.
- Y. Hou, Y. Chen, Y. Xue, Y. Zheng and L. Jiang, Water collection behavior and hanging ability of bioinspired fiber, *Langmuir*, 2012, **28**, 4737–4743.
- P. Contal, J. Simao, D. Thomas, T. Frising, S. Calle, J. C. Appert-Collin and D. Bemer, Clogging of Fibre Filters by submicron droplets. Phenomena and influence of operating conditions, *Aerosol Sci.*, 2004, **35**, 263–278.
- S. U. Patel and G. G. Chase, Separation of water droplets from water-in-diesel dispersion using superhydrophobic polypropylene fibrous membranes, *Sep. Purif. Technol.*, 2014, **126**, 62–68.
- D. Kampa, S. Wurster, J. Buzengeiger, J. Meyer and G. Kasper, Pressure drop and liquid transport through coalescence filter media used for oil mist filtration, *Int. J. Multiph. Flow*, 2014, **58**, 313–324.
- J. Song, S. Huang, Y. Lu, X. Bu, J. E. Mates, A. Ghosh, R. Ganguly, C. J. Carmalt, I. P. Parkin, W. Xu and C. M. Megaridis, Self-Driven One-Step Oil Removal from Oil Spill on Water via Selective-Wettability Steel Mesh, *ACS Appl. Mater. Interfaces*, 2014, **6**, 19858–19865.
- B. Ramos-Alvarado, J. D. Sole, A. Hernandez-Guerrero and M. W. Ellis, Experimental characterization of the water transport properties of PEM fuel cells diffusion media, *J. Power Sources*, 2012, **218**, 221–232.
- L. Hao and P. Cheng, Lattice Boltzmann simulations of water transport in gas diffusion layer of a polymer electrolyte membrane fuel cell, *J. Power Sources*, 2010, **195**, 3870–3881.
- R. Hanumanthu and K. J. Stebe, Equilibrium shapes and locations of axisymmetric, liquid drops on conical, solid surfaces, *Colloids Surfaces A Physicochem. Eng. Asp.*, 2006, **282–283**, 227–239.
- G. McHale, M. Newton and B. Carroll, The Shape and Stability of Small Liquid Drops on Fibers, *Oil Gas Sci. Technol. – Rev. IFP*, 2001, **56**, 47–54.
- G. McHale and M. I. Newton, Global geometry and the equilibrium shapes of liquid drops on fibers, *Colloids Surfaces A Physicochem. Eng. Asp.*, 2002, **206**, 79–86.
- H. B. Eral, G. Manukyan and J. M. Oh, Wetting of a drop on a sphere, *Langmuir*, 2011, **27**, 5340–5346.
- R. De Ruiter, J. De Ruiter, H. B. Eral, C. Semperebon, M. Brinkmann and F. Mugele, Buoyant droplets on functional fibers, *Langmuir*, 2012, **28**, 13300–13306.
- T. H. Chou, S. J. Hong, Y. E. Liang, H. K. Tsao and Y. J. Sheng, Equilibrium phase diagram of drop-on-fiber: Coexistent states and gravity effect, *Langmuir*, 2011, **27**, 3685–3692.
- A. Milchev and K. Binder, Polymer nanodroplets adsorbed on nanocylinders: A Monte Carlo study, *J. Chem. Phys.*, 2002, **117**, 6852–6862.
- M. M. Amrei, M. Davoudi, G. G. Chase and H. V. Tafreshi, Effects of roughness on droplet apparent contact angles on a fiber, *Sep. Purif. Technol.*, 2017, **180**, 107–113.
- B. J. Mullins, I. E. Agranovski, R. D. Braddock and C. M. Ho, Effect of fiber orientation on fiber wetting processes, *J. Colloid Interface Sci.*, 2004, **269**, 449–458.
- A. Bick, F. Boulogne, A. Sauret and H. A. Stone, Tunable transport of drops on a vibrating inclined fiber, *Appl. Phys. Lett.*, 2015, **107**, 181604.
- B. J. Mullins, A. Pfrang, R. D. Braddock, T. Schimmel and G. Kasper, Detachment of liquid droplets from fibres- Experimental and theoretical evaluation of detachment force due to interfacial tension effects, *J. Colloid Interface Sci.*, 2007, **312**, 333–340.
- C. J. Hotz, R. Mead-Hunter, T. Becker, A. J. C. King, S. Wurster, G. Kasper and B. J. Mullins, Detachment of droplets from cylinders in flow using an experimental analogue, *J. Fluid Mech.*, 2015, **771**, 327–340.
- R. P. Sahu, S. Sinha-Ray, A. L. Yarin and B. Pourdeyhimi, Blowing drops off a filament, *Soft Matter*, 2013, **9**, 6053–6071.
- M. Davoudi, J. Fang and G. G. Chase, Barrel shaped droplet movement at junctions of perpendicular fibers with different orientations to the air flow direction, *Sep. Purif. Technol.*, 2016, **162**, 1–5.
- M. M. Amrei, D. G. Venkateshan, J. Atulasimha and H. V. Tafreshi, Novel Approach to Measure Droplet Detachment Force from Fibers, *Langmuir*, 2016, **32**, 13333–13339.
- S.-G. Kim and W. Kim, Drop impact on a fiber, *Phys. Fluids*, 2016, **28**, 042001–042009.
- E. Dressaire, A. Sauret, F. Boulogne and H. A. Stone, Drop

- impact on a flexible fiber, *Soft Matter*, 2016, **12**, 200–208.
- 28 F. Ito, S. Komatsubara, N. Shigezawa, H. Morikawa, Y. Murakami, K. Yoshino and S. Yamanaka, Mechanics of water collection in plants via morphology change of conical hairs, *Appl. Phys. Lett.*, 2015, **106**, 133701–133704.
- 29 F. Weyer, M. Lismont, L. Dreesen and N. Vandewalle, Compound droplet manipulations on fiber arrays, *Soft Matter*, 2015, **11**, 7086–7091.
- 30 J. R. Choudhuri, D. Vanzo, P. A. Madden, M. Salanne, D. Bratko and A. Luzar, Dynamic Response in Nanoelectrowetting on a Dielectric, *ACS Nano*, 2016, **10**, 8536–8544.
- 31 W. Humphrey, A. Dalke and K. Schulten, VMD: visual molecular dynamics., *J. Mol. Graph.*, 1996, **14**, 33–8, 27–8.
- 32 P. Mark and L. Nilsson, Structure and Dynamics of the TIP3P, SPC, and SPC/E Water Models at 298 K, *J. Phys. Chem. A*, 2001, **105**, 9954–9960.
- 33 H. J. C. Berendsen, J. R. Grigera and T. P. Straatsma, The missing term in effective pair potentials, *J. Phys. Chem.*, 1987, **91**, 6269–6271.
- 34 T. Werder, J. H. Walther, R. L. Jaffe, T. Halicioglu and P. Koumoutsakos, On the Water–Carbon Interaction for Use in Molecular Dynamics Simulations of Graphite and Carbon Nanotubes, *J. Phys. Chem. B*, 2003, **107**, 1345–1352.
- 35 D. Vanzo, D. Bratko and A. Luzar, Tunable wetting of surfaces with ionic functionalities, *J. Phys. Chem. C*, 2012, **116**, 15467–15473.
- 36 J. Driskill, D. Vanzo, D. Bratko and A. Luzar, Wetting transparency of graphene in water, *J. Chem. Phys.*, 2014, **141**, 18C517-8.
- 37 N. Giovambattista, A. B. Almeida, A. M. Alencar and S. V Buldyrev, Validation of capillarity theory at the nanometer scale by atomistic computer simulations of water droplets and bridges in contact with hydrophobic and hydrophilic surfaces, *J. Phys. Chem. C*, 2016, **120**, 1597–1608.
- 38 D. Bratko, C. D. Daub, K. Leung and A. Luzar, Effect of field direction on electrowetting in a nanopore, *J. Am. Chem. Soc.*, 2007, **129**, 2504–2510.
- 39 C. D. Daub, D. Bratko and A. Luzar, Electric control of wetting by salty nanodrops: Molecular dynamics simulations, *J. Phys. Chem. C*, 2011, **115**, 22393–22399.
- 40 S. Sharma and P. G. Debenedetti, Free energy barriers to evaporation of water in hydrophobic confinement, *J. Phys. Chem. B*, 2012, **116**, 13282–13289.
- 41 N. Giovambattista, P. G. Debenedetti and P. J. Rossky, Effect of surface polarity on water contact angle and interfacial hydration structure, *J. Phys. Chem. B*, 2007, **111**, 9581–9587.
- 42 V. Molinero and E. B. Moore, Water modeled as an intermediate element between carbon and silicon, *J. Phys. Chem. B*, 2009, **113**, 4008–4016.
- 43 M. H. Factorovich, V. Molinero and D. A. Scherlis, Hydrogen-Bond Heterogeneity Boosts Hydrophobicity of Solid Interfaces, *J. Am. Chem. Soc.*, 2015, **137**, 10618–10623.
- 44 V. R. Ardham and F. Leroy, Thermodynamics of atomistic and coarse-grained models of water on nonpolar surfaces, *J. Chem. Phys.*, 2017, **147**, 74702–12.
- 45 L. Lupi, N. Kastelowitz and V. Molinero, Vapor deposition of water on graphitic surfaces: Formation of amorphous ice, bilayer ice, ice I, and liquid water, *J. Chem. Phys.*, 2014, **141**, 18–508.
- 50 S. Plimpton, Fast Parallel Algorithms for Short – Range Molecular Dynamics, *J. Comput. Phys.*, 1995, **117**, 1–19.
- 51 D. J. Evans and B. L. Holian, The Nose–Hoover thermostat, *J. Chem. Phys.*, 1985, **83**, 4069–4074.
- 52 H. B. Eral, J. de Ruiter, R. de Ruiter, J. M. Oh, C. Semperebon, M. Brinkmann and F. Mugele, Drops on functional fibers: from barrels to clamshells and back, *Soft Matter*, 2011, **7**, 5138.
- 53 H. Aziz, N. M. Farhan and H. Vahedi Tafreshi, Effects of fiber wettability and size on droplet detachment residue, *Exp. Fluids*, 2018, **59**, 122.
- 54 U. Moseler, M. & Landman, Formation, Stability, and Breakup of Nanojets, *Science (80-.)*, 2000, **289**, 1165–1169.
- 55 N. Gopan and S. P. Sathian, Rayleigh instability at small length scales, *Phys. Rev. E*, 2014, **90**, 33001.
- 56 A. Tiwari and J. Abraham, Dissipative particle dynamics simulations of liquid nanojet breakup, *Microfluid. Nanofluidics*, 2008, **4**, 227–235.
- 57 D. K. Bhuptani and S. P. Sathian, Effect of axial electric field on the Rayleigh instability at small length scales, *Phys. Rev. E*, 2017, **95**, 053115–053126.
- 58 N. Gopan and S. P. Sathian, A Langevin dynamics study of nanojets, *J. Mol. Liq.*, 2014, **200**, 246–258.
- 59 R. Tadmor, R. Das, S. Gulec, J. Liu, H. E. N’guessan, M. Shah, P. S Wasnik and S. B. Yadav, Solid-Liquid Work of Adhesion, *Langmuir*, 2017, **33**, 3594–3600.
- 60 É. Lorenceau, C. Clanet and D. Quéré, Capturing drops with a thin fiber, *J. Colloid Interface Sci.*, 2004, **279**, 192–197.
- 61 T. Werder, J. H. Walther, R. L. Jaffe, T. Halicioglu and P. Koumoutsakos, On the water-carbon interaction for use in molecular dynamics simulations of graphite and carbon nanotubes, *J. Phys. Chem. B*, 2003, **107**, 1345–1352.
- D. Vanzo, D. Bratko and A. Luzar, Wettability of pristine and alkyl-functionalized graphane, *J. Chem. Phys.*, 2012, **137**, 34707–18.
- M. Sellier, J. W. Grayson, L. Renbaum-Wolff, M. Song and A. K. Bertram, Estimating the viscosity of a highly viscous liquid droplet through the relaxation time of a dry spot, *J. Rheol. (N. Y. N. Y.)*, 2015, **59**, 733–750.
- B. Li, V. Vivacqua, M. Ghadiri, Z. Sun, Z. Wang and X. Li, Droplet deformation under pulsatile electric fields, *Chem. Eng. Res. Des.*, 2017, **127**, 180–188.
- W. Kang and U. Landman, Universality crossover of the pinch-off shape profiles of collapsing liquid nanobridges in vacuum and gaseous environments., *Phys. Rev. Lett.*, 2007, **98**, 064504–064508.



TOC: For all drop sizes, the water residue on the fiber is maximized by using intermediate rates of forcible drop detachment.